THERMOGRAPHIC PHOSPHORS AS A MEANS OF ESTIMATING HEATING RATE TO SOLVE THE INVERSE HEAT CONDUCTION PROBLEM

By

Paul R. Crim

Thesis

Submitted to the Faculty of the

Graduate School of Vanderbilt University

in partial fulfillment of the requirements

for the degree of

MASTER OF SCIENCE

in

Mechanical Engineering

December, 2005

Nashville, Tennessee

Approved:

Professor D. Greg Walker

Professor Mark A. Stremler

Professor Alvin M. Strauss

ACKNOWLEDGEMENTS

I would like to express my gratitude to the Vanderbilt University School of Engineering, the Department of Mechanical Engineering, and the Vanderbilt University Discovery Grant program, and for the IBM Fellowship for financial support. I would like to thank Oak Ridge National Laboratory for lending expertise and equipment, and specifically Steve Allison for all the help he gave me in understanding thermographic phosphors. I would especially like to thank my advisor, Professor Greg Walker, without whose help this never would have been possible. Additionally, I would like to thank all friends and family who have supported me during my tenure at Vanderbilt. Thank you God for the opportunities. Mom, Dad, Joel, Nan, and Ann, thank you.

TABLE OF CONTENTS

LIST OF TABLES

LIST OF FIGURES

LIST OF ABBREVIATIONS

T	temperature	°C
t	time	s
ξ	dimensionless time	
I	emission intensity	V
I_0	initial emission intensity	V
n^*	number of excited luminescence centers	
W_R	transition rate of radiative mechanisms	s^{-1}
W_{NR}	transition rate of non-radiative mechanisms	s^{-1}
τ	decay time	s
τ_0	initial decay time	s
Y	discrete temperature measurements	°C
Λ	discrete heating rate measurements	°C/s
k	geometry based constant	m^2 °C / W s
H	dimensionless heating rate	
Q	heat flux	W/m^2
θ	dimensionless temperature	
L	dimensionless length	
α	thermal diffusivity	m^2/s

CHAPTER I

INTRODUCTION

Heat flux is the flow of heat per unit area from a higher temperature to a lower temperature which occurs when a temperature gradient exists [Holman, 2002]. Given the proper heat flux boundary and initial conditions, the temperature history can be solved stably. However, the process of solving for heat flux given a known temperature history is more involved. The lack of stability and accuracy in current methods of heat flux determination leads to the need for and investigation of alternative methods of heat flux determination. Currently the two categories of heat flux determination are direct measurement and data reduction. The direct measurement techniques can be simplified into four categories: 1) differential temperature, 2) calorimetric methods, 3) energy supply or removal, and 4) mass transfer analogy [Childs et al., 1999]. Although the differential temperature method is the most common in direct measurement, constraints on size, cost, and sensitivity prohibit any one method from being suitable for all applications. The method of differential temperature uses multiple thermocouples or thermopiles to measure temperature gradients. The simplest differential temperature heat flux gage is the layered gage. Thermocouples measure the temperature on both sides of a thermal resistance layer, and the temperature gradient is proportional to the heat flux [Diller, 1993]. The gage must be calibrated depending on the materials used and the range of temperatures and heat fluxes in the application. These devices are typically expensive and difficult to calibrate [Childs et al., 1999]. Furthermore, they generally have a slow response time and can integrate high-frequency components in the data [Crim et al., 2004].

The second approach to determining heat flux is to use data reduction techniques to estimate heat flux from temperature measurements. While temperature measurements are inexpensive and reliable, the data reduction of temperature measurements to solve for heat flux is ill-posed. The method of data reduction involves

the inverse heat conduction problem, which is inherently ill-posed and amplifies any noise and uncertainty in the measurements during the data reduction. However, it can be shown that by using measurements of heating rate, which is defined as the first time derivative of temperature, instead of temperature measurements, the solution to the inverse heat conduction problem becomes more stable with less error[Walker, 2005]. This leads to the need for a viable method of measuring heating rate directly. It is the aim of this thesis to show that it is possible to measure both temperature and heating rate simultaneously using thermographic phosphors. The experiment uses a tungsten filament to heat the phosphor over 200°C in one second. An LED is used to excite the phosphor, and the phosphor emission is recorded by a photomultiplier tube. The intensity measurements are used in a curve fitting technique to extract temperature dependent properties of the phosphor. The results of the experiment show that thermographic phosphors can be used to estimate heating rate.

CHAPTER II

THEORY

Inverse Heat Transfer

Interest in the inverse heat transfer problem has grown over the past century. Although interest in the solution to the inverse problem dates back to the early 1900's [Tikhonov and Arsenin, 1977], one of the major recent issues to spark such interest was the space program in the 1950's and 1960's. The issue of aerodynamic heating on the surface of the space shuttle during reentry was the focus of concern [Ozisik and Orlande, 2000]. The heating on the surface of the space shuttle is so great that direct temperature measurement is impossible due to the survivability of the measurement devices. However, temperature measurements could easily be made on the inner surface of the shuttle's insulation, where the temperature is much lower, and those temperature measurements are used to estimate the outer surface temperature.

A typical heat transfer problem contains some known boundary conditions, initial conditions, and physical properties, and the problem calls for the solution to some unknown temperature distribution. In general, the causal properties are known and the problem is solved for some effect of the causal properties. In the inverse problem, the effect can be measured and is used to estimate one of the causal properties [Ozisik and Orlande, 2000]. In the inverse heat conduction problem, which is of interest in the present work, the temperature is the effect that can be measured, and the boundary heat flux is unknown and must be estimated.

Although advances have been made in the solution to the inverse heat transfer problem, mathematically the problem is ill-posed. There are three conditions that set apart an ill-posed problem from a well-posed problem. The three conditions that make a problem well-posed are: 1) the solution must exist, 2) the solution must be unique, and 3) the solution must be stable under small changes to the input data

[Kress, 1989]. The first condition is satisfied in the inverse heat conduction problem by intuition, such that if the measured temperature increases, there must be some heat flux causing the temperature gradient. Mathematically, the second condition cannot be proven for all inverse problems, so not all inverse problems are well-posed [Ozisik and Orlande, 2000]. Finally, the inverse heat conduction problem is very sensitive to small random error in the temperature measurements, so at the very least the problem is ill-posed for violating the stability condition [Beck et al., 1985].

Using the inverse heat conduction problem to estimate heat flux from temperature measurements involves a Volterra equation of the first kind. In a Volterra equation of the first kind, the heat flux term is inside an integral, therefore mathematically, the error in the solution is unbounded. The equation must be differentiated to remove the heat flux term from within the integral, and much of the difficuly in determining heat flux from temperature measurements comes from the differentiation of data [Ehrich, 1954]. The equation

$$Y(t) = \int_0^t k(t,t')Q(t')dt' \tag{1}$$

is an example of a Volterra equation of the first kind, where Y is discrete temperature data to be integrated. Q is the heat flux and k is a known kernel dependent on the geometry of the problem. In an attempt to stabilize the solution to the inverse heat conduction problem, Frankel and Keyhani [1997] introduced the idea of using temperature derivatives rather than temperature measurements. Using heating rate measurements to solve the inverse heat conduction problem for heat flux involves using a Volterra equation of the second kind, which takes the form

$$\frac{dY(t)}{dt} = \Lambda(t) = Q(t) - \int_0^t \frac{\partial k(t,t')}{\partial t} Q(t')dt'. \tag{2}$$

Volterra equations of the second kind are inherently more stable than Volterra equations of the first kind [Kress, 1989]. Here Λ is the measured heating rate. Recall that

the third condition of a well-posed problem is stability of the solution under small changes to the input data. By using a more stable equation to estimate heating rate, the process becomes more robust, and small changes to the input have less of an effect on the heat flux solution. Therefore, the method of using heating rate instead of temperature as the input to the inverse heat conduction problem solves the violation of the third condition of a well-posed problem. The following example presents solutions to the inverse heat conduction problem using temperature measurements and heating rate measurements.

Walker [2005] simulates a one dimensional heating problem to show the advantages of measuring heating rate rather than temperature. In the problem, the heat flux enters one side of a slab of length L, and the boundary condition on the other side of the slab is constant temperature. The heat flux, temperature, and time in the problem are dimensionless, and ξ is the symbol used for dimensionless time, where $\xi = t\alpha/L^2$. A square heat flux is introduced, with an amplitude of unity, starting at ξ=0.2 and ending at ξ=0.8. A solution for temperature is made for the forward conduction probem. To simulate actual temperature measurements, random noise is added to the exact temperature solution (Y_n), and both are displayed in figure 1.

The forward conduction problem is also solved for heating rate, and random noise is added to that solution to simulate heating rate measurements. The simulated heating rate measurements (H_n) and exact heating rate solution (Λ) are then compared to the differentiated temperature measurements (H_d) in figure 2. The simulated temperature measurements are used to solve the inverse heat conduction problem to estimate heat flux, and the heat flux solution (Q_{Y_n}) is compared to the square heat flux (Q) in figure 3. The heat flux is then estimated using the simulated heating rate measurements (Q_{H_n}) and heating rate from differentiated temperature measurements (Q_{H_d}) in the inverse heat conduction problem, and the comparison with actual heat flux is shown in figure 4. Comparing figures 3 and 4, the solution for heat flux from heating rate meaurements is more stable than the solution using temperature measurements.

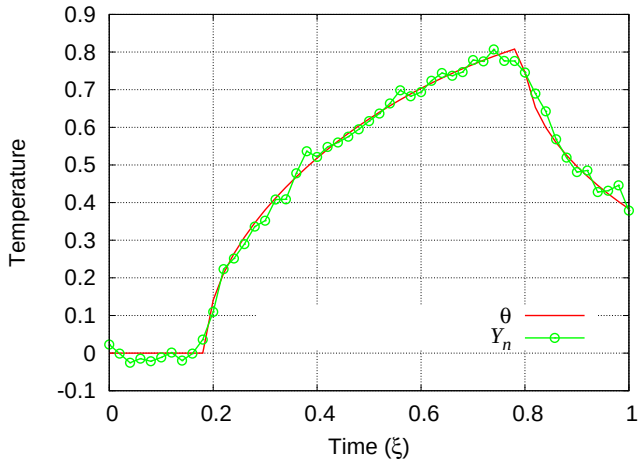

Figure 1: Exact Temperature Solution and Simulated Temperature Measurement for Square Heat Flux

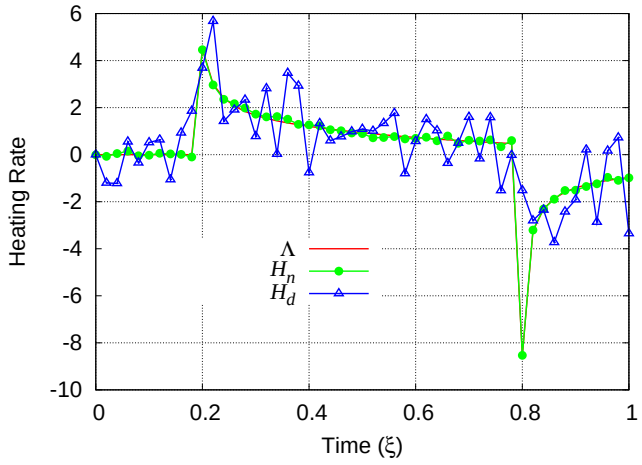

Figure 2: Exact Heating Rate Solution, Simulated Heating Rate Measurement, and Heating Rate from Numerically Differentiated Temperature Measurements for Square Heat Flux

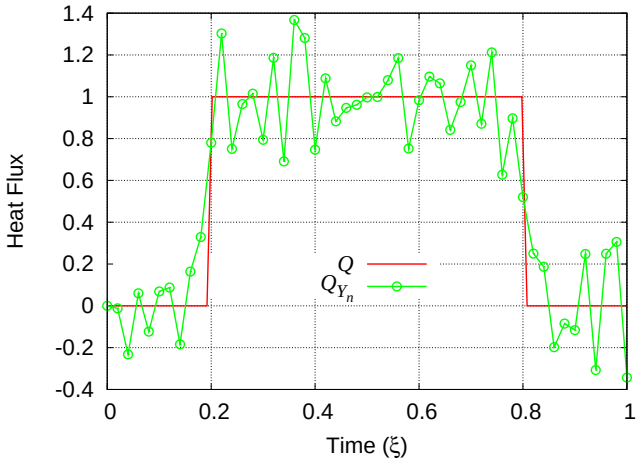

Figure 3: Original Square Heat Flux and Heat Flux Solution to IHCP Using Simulated Temperature Measurements

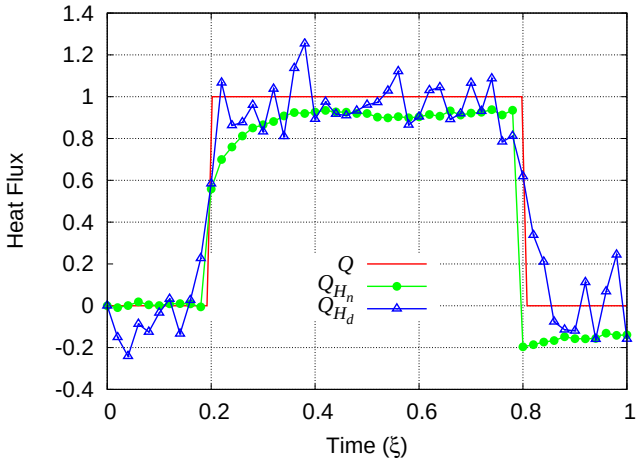

Figure 4: Original Square Heat Flux, Heat Flux Solution Using Measured Heating Rate, and Heat Flux Solution Using Heating Rate From Differentiated Measured Temperature

The need for a means of measuring heating rate directly to improve estimates of the solution to the inverse heat conduction problem emerges from this problem. The need for heating rate measurement devices has been identified in conference proceedings [Frankel and Keyhani, 1999, Frankel and Osborne, 2003]. The present work examines thermographic phosphors as a means of measuring heating rate.

Thermographic Phosphors

Walker and Schetz [2003] first identified thermographic phosphors as a potential means of measuring heating rate. Thermographic phosphors are rare earth-doped ceramics that fluoresce when exposed to light. The emission wavelength, intensity, and decay rate are all temperature dependent, so any of these properties can be measured to determine temperature. Although thermographic phosphors are generally used for steady-state temperature applications, emission is inherently transient, so intensity measurements can also be used to extract transient temperature data, such as heating rate. The type of phosphor used and the measurement technique are generally chosen based on the application and data requirements [Allison and Gillies, 1997].

When incident photons excite a phosphor, it begins to reemit at a specific wavelength determined by its electronic band structure [Shionoya and Yen, 1999]. Many factors contribute to the intensity of the phosphor emission, such as material properties, doping, temperature, and excitation source. The measured emission intensity I is proportional to the rate of change of excited luminescence centers n^* [Shionoya and Yen, 1999], such that

$$I \propto \frac{dn^*}{dt}. \tag{3}$$

The number of luminescence centers (electron/hole pairs available for recombination) is governed by the radiative and non-radiative recombination of electrons with holes

as

$$\frac{dn^*}{dt} = -(W_R + W_{NR})n^*, \tag{4}$$

where W is the transition rate of radiative and non-radiative mechanisms, and the negative sign indicates emission. The transition rates are usually treated as a single term, known as the overall lifetime, τ, such that [Shionoya and Yen, 1999]

$$\tau^{-1} = W_R + W_{NR}. \tag{5}$$

In general, this lifetime is temperature dependent. When the excitation source is removed, the number of excited electrons n is governed by the differential equation

$$\tau(T)\frac{dn}{dt} + n = 0, \tag{6}$$

where $\tau[T(t)]$ is the electron lifetime, which is a function of temperature that can change in time. Assuming the electron lifetime is constant during the decay, the solution to equation 6 is given as

$$\frac{n}{n_0} = \exp\left(-\frac{t}{\tau}\right), \tag{7}$$

where n_0 is the number of electrons at $t = 0$, which is when the excitation source is removed. By differentiating equation 7 and recalling equation 3, the intensity can be expressed in terms of the decay time as

$$\frac{I}{I_0} = \exp\left(-\frac{t}{\tau}\right). \tag{8}$$

This equation is known as the standard model, where I_0 is the initial emission intensity when the excitation source is removed, at time $t = 0$.

The standard model is used to describe phosphor emission intensity decay in non-contact thermometry. If the temperature is constant, then the decay time τ, which is a function of temperature, also remains constant. In this case, the

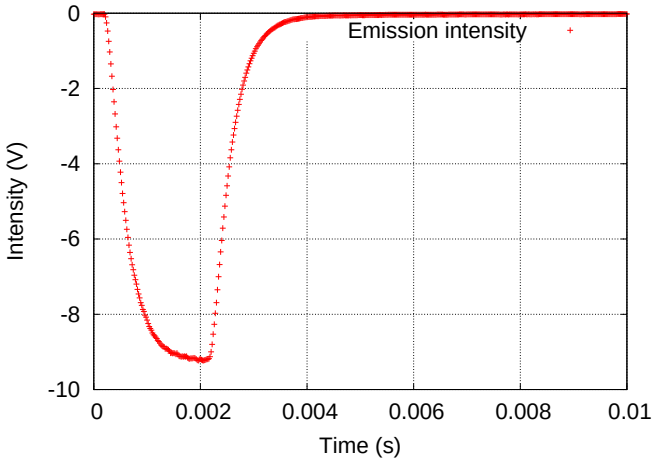

Figure 5: Phosphor Emission Intensity

emission intensity of a phosphor at a given temperature is recorded, and the decay time is extracted from the emission data. This decay time is specific to a certain temperature, and the relationship between decay time and temperature is given in the calibration curve. To execute non-contact thermometry using thermographic phosphors, an excitation source, which is usually an LED or laser, and a device to record the emission intensity, such as a photomultiplier tube or photo diode, are required. The excitation source is controlled by a function generator, which pulses the light source at a specified frequency and duty cycle. Figure 5 shows the emission intensity of europium-doped lanthanum oxysulfide, La_2O_2S:Eu, excited by an LED pulsed at 100 Hz with a 20% duty cycle, with the emission data recorded by a photomultiplier tube at 50,000 Hz. The emission amplitude is negative because photomultiplier tubes return a negative voltage when converting light to voltage. The area of interest in figure 5 is the decay of the emission, between 0.0023 seconds and 0.0035 seconds. The decay curve in this area is defined by the standard model (equation 8). The unknown parameters I_0 and τ can be determined using curve fitting techniques. There are two common approaches that can be performed on the emission decay data. The simpler method is to convert the standard model from an exponential to a linear equation. This is accomplished by taking the natural logarithm of both sides of equation 8,

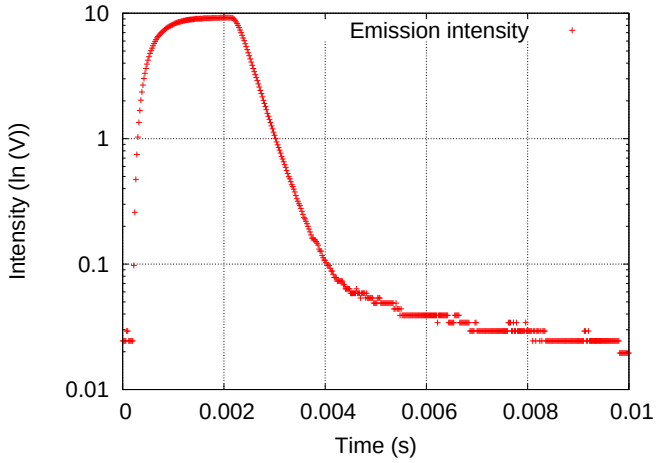

Figure 6: Exponential Phosphor Emission Decay Curve Converted to Linear Straight Line

which results in

$$ln(I) = ln(I_0) - \frac{1}{\tau}t. \tag{9}$$

Equation 9 takes the form of a linear equation $y = mx + b$ by setting $ln(I) = y$, $ln(I_0) = b$, $-1/t = m$, and $t = x$. Figure 6 shows the converted data from figure 5. Beyond t=0.0035 seconds, the line begins to curve, indicating that at this point the plot is no longer a simple exponential. This deviation arises from the noise in the signal and an offset inherent to the measurement system. Only the section of the graph where the line is straight is to be considered in the curve fit. Because this view makes it easier to see the bounds of the simple exponential, it is often desirable to use this view to set the limits of the curve fit when using an exponential curve fit. A linear regression of the straight line results in values for I_0 and τ.

The other method is to use a non-linear curve fitting method to fit the exponential curve to the standard model. Although this method is more computationally intensive, it is also more rigorous. The decay model in equation 8 is modified to include an added offset term to account for the photomultiplier tube. The phosphor emission decays to zero, but the photomultiplier tube adds a small signal, which must be accounted for in the equation. The dark current in the photomultiplier tube

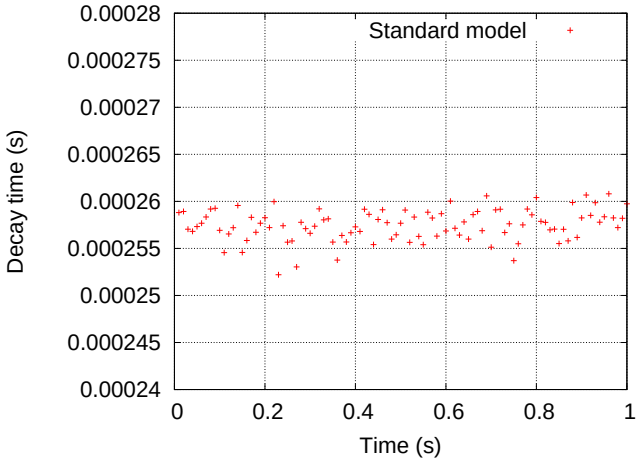

Figure 7: Decay Time of 100 Pulses of La_2O_2S:Eu at 190°C

results in an offset voltage of 5mV. An entire set of data generally includes multiple pulses, each with a separate decay curve. Any noise in the data causes errors in the results for decay time. A final decay time for the experiment is determined by averaging the decay time from each pulse in the experiment (see figure 7).

Because each phosphor has different properties, a new calibration for each phosphor must be generated. Furthermore, many phosphors emit at more than one wavelength. This means that a phosphor may emit at a low frequency for a lower temperature range and at a higher frequency for a higher temperature range. For example, the 630nm band of the phosphor used in figure 5 has a decay time of the order of 100μs, and it is temperature sensitive in the range of 170°C $< T <$ 210°C. Different phosphors have a wide range of decay times and temperature ranges, so a single phosphor may have multiple calibration curves. A calibration curve is created by heating a phosphor to a known temperature and then determining a decay time from a curve fit. This process is repeated at various steady-state temperatures until the calibration curve is complete, which occurs when a minimum sensitivity is reached [Allison and Gillies, 1997]. Figure 7 shows the results of an exponential curve fit of La_2O_2S:Eu at 190°C. The phosphor was heated to 190°C, and an LED was pulsed at 100Hz with a 20% duty cycle. Emission data was recorded for one second, and each

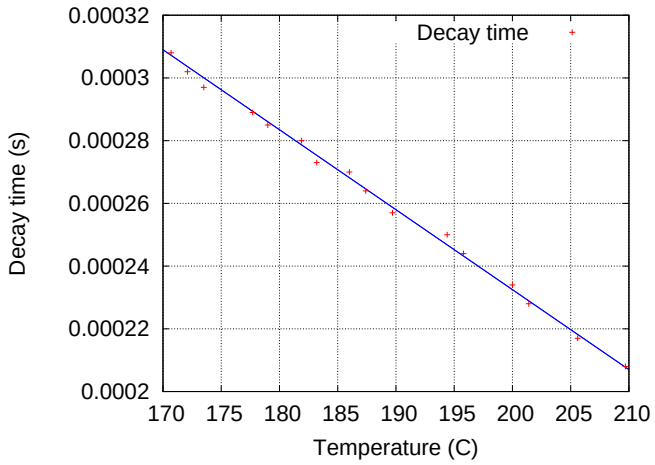

Figure 8: Calibration Curve for 630nm Band of La_2O_2S:Eu

of the 100 decay curves was fit to the standard model. The average of the 100 values of τ was 0.000257 seconds, which then became a point on the calibration curve. The standard deviation of the averaged decay time is 0.00000167s, which is less than one percent of the value of decay time, so the error bars are not shown in the plot of the calibration curve. This process was repeated incrementally from 170°C to 210°C to create the calibration curve, shown in figure 8.

Under transient conditions, where the temperature transients are of the order of the decay time, the assumption of constant decay time is no longer valid. The standard model cannot predict an accurate value for τ if the temperature change is significant over the decay curve. If the decay time does change over the emission decay, then τ must be expressed as a function of time. The simplest approximation is to assume that the decay time is a linear function of time and to use a first order Taylor series expansion of the decay time, so that

$$\tau(t) = \tau_0 + \frac{d\tau}{dt}t + O(t^2), \tag{10}$$

where τ_0 is the decay time at the beginning of the decay, at $t = 0$. The Taylor series expansion of τ is substituted into the governing equation (equation 6), and the

solution for intensity to that differential equation is [Crim et al., 2004]

$$\frac{I}{I_0} = \left(\frac{\tau_0}{\tau_0 + \frac{d\tau}{dt} t} \right)^{1/\frac{d\tau}{dt}}. \tag{11}$$

Equation 11 is the power model, where I_0 and τ_0 are the intensity and decay time at time $t = 0$. This new model contains a transient term, $\mathrm{d}\tau/\mathrm{dt}$, which accounts for any change in the decay time over the emission decay. This new term, known as the decay time rate, is an additional parameter that can be extracted from the decay curve using a curve fit. Notice that for small temperature changes, where $\mathrm{d}\tau/\mathrm{dt} \rightarrow 0$, the power model is singular. This leads to the need for a second transient model. Walker and Schetz [2003] suggest an alternate model which retains the exponential approximation, but treats the decay time as a linearly varying function of temperature. As a result, decay time is approximated as a truncated Taylor series and substituted directly into the standard model. The resulting equation is

$$\frac{I}{I_0} = \exp\left(-\frac{t}{\tau_0 + \frac{1}{2}\frac{d\tau}{dt} t} \right), \tag{12}$$

known as the exponential model. Because the Taylor series is substituted directly into the standard model, it does not satisfy the governing equation. Therefore, the power model and exponential model were set equal and solved in terms of decay time rate ($\mathrm{d}\tau/\mathrm{dt}$). This led to the addition of a $\frac{1}{2}$ term in the denominator of the exponential term in the exponential model. Notice that as $\mathrm{d}\tau/\mathrm{dt} \rightarrow 0$, the exponential model reduces to the standard model. By fitting emission decay data to the exponential and power models, both decay time τ and the decay time rate $\mathrm{d}\tau/\mathrm{dt}$ can be extracted from phosphor emission data. The decay time is used to determine the temperature at each pulse, and the decay time rate is used to determine the heating rate. The heating rate can be found directly using the chain rule, where

$$\frac{dT}{dt} = \frac{dT}{d\tau}\frac{d\tau}{dt}. \tag{13}$$

The term $dT/d\tau$ is found using the calibration curve (figure 8). Recall from figure 8 that the calibration curve gives the relationship between temperature and decay time for a given emission band of a phosphor. $dT/d\tau$ is recovered by differentiating the calibration curve and taking the inverse of that value. The heating rate is then determined by taking the product of $dT/d\tau$ from the calibration curve and $d\tau/dt$ from the curve fit.

CHAPTER III

EXPERIMENT

The experiment consists of two parts. The first part takes place under steady-state conditions, where the phosphor is heated to different steady-state temperatures and the decay time is recorded. The final result of this part of the experiment is the calibration curve. The second part of the experiment takes place under transient conditions, where the phosphor is heated and the decay time and decay time rate are recorded. The final result of this part of the experiment is the heating rate of phosphor.

The experimental setup is almost identical for the two parts of the experiment. The only difference between the two setups is the method of heating the phosphor. For the steady state part, the phosphor is painted onto a thin, square sheet of aluminum, measuring 25mm x 25mm x 1mm. For the transient part, the phosphor is painted onto a tungsten filament. In order to paint the phosphor onto a surface, the phosphor, which is in powder form, is mixed with water and a ceramic binder. The mixture contains 40% phosphor, 30% distilled water, and 30% Resbond^{TM} ceramic binder. This mixture is then painted onto a clean, dry surface using an airbrush. The phosphor should be painted as a thin coat, so that the thermal properties of the phosphor have a minimal effect on the experiment. Extra coats of the phosphor do not have a significant effect on the emission intensity. Once painted, the surface must cure for twenty-four hours at room temperature.

The temperature range of interest for this experiment is $170°\text{C} < T < 210°\text{C}$, which corresponds to an excitation wavelength of 350 nm and an emission wavelength of 630 nm for the phosphor La_2O_2S:Eu. A pulse generator controls a 350 nm LED, which is the excitation source. A photomultiplier tube, which is contained in an aluminum housing to shield it from electrical and optical disturbances, is fitted with a 630 nm bandwidth filter to isolate the phosphor emission. The photomultiplier

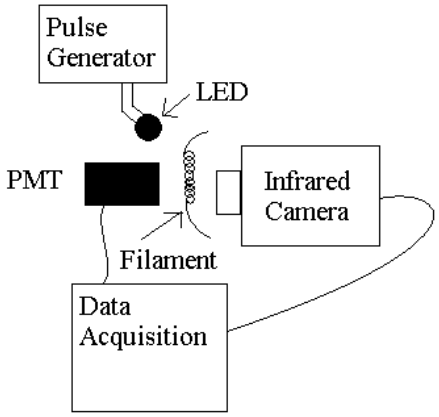

Figure 9: Schematic of Experimental Setup

Table 1: List of Equipment

Equipment	Name & Model Number
Power Supply	Global Specialties Instruments 1315 AC/DC Power Supply
Pulse Generator	DEI PDG-2510 Digital Delay/Pulse Generator
Oscilloscope	Tektronix TDS 2012 2 Channel Digital Storage Oscilloscope
Photomultiplier Tube	Hamamatsu H5783 Photosensor Module
Infrared Thermal Imaging Camera	Mikron Thermo Tracer TS7302

tube is connected to an oscilloscope and a computer, which handles the data acquisition. An infrared thermal imaging camera is focused on the phosphor to read the temperature during experimentation. Figure 9 shows a schematic of the experimental setup, and figure 10 shows a picture of the setup.

In the steady state portion of the experiment, the phosphor is heated to an initial temperature of 170°C with the strip heater. The pulse generator is set to pulse the LED at 100 Hz with a 20% duty cycle. Figure 11 shows three pulses of the LED (top) and the phosphor emission (bottom). In order to achieve best results, the experiment must take place in a dark room, with as little ambient light

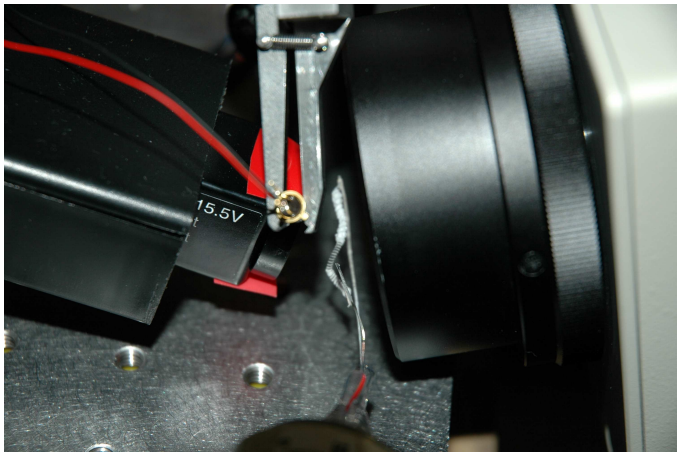

Figure 10: Experimental Setup

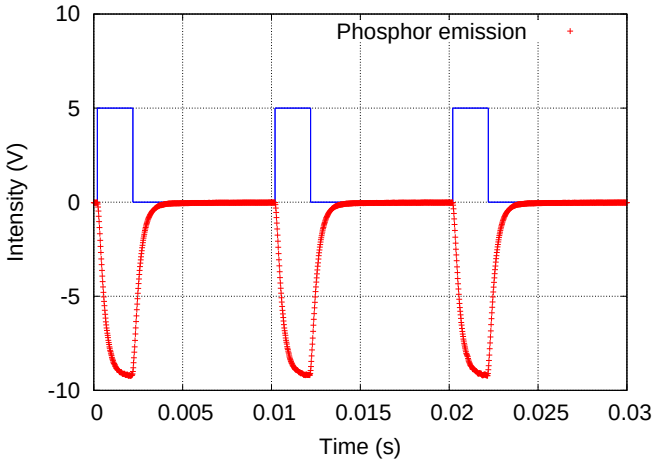

Figure 11: LED and Phosphor Emission Pulses

as possible. To maximize the emission signal passed from the photomultiplier tube to the data acquisition, it is necessary to minimize the distance from the LED and the photomultiplier tube to the phosphor. When the phosphor reaches a constant temperature, measured by the thermal imaging camera, the phosphor emission data is recorded for approximately one second. One second of data at 100 Hz yields 100 values for decay time, which is a sufficient number to minimize any error due to noise by averaging. Recall figure 7, where the values for decay time at 190°C vary between 255μs and 260μs. Because the temperature is constant, the decay time, which is a function of temperature, should also be constant. This variance is caused by noise in the data recorded by the photomultiplier tube, and the effect of the noise can be minimized by averaging the decay time results. This process is then repeated incrementally from 170°C to 210°C. The final results are plotted in the calibration curve, which is seen in figure 8.

To perform transient tests, a tungsten filament was coated with phosphor to be used as a heating source. The filament is connected to a variable voltage power supply. The power supply is adjusted to the desired setting and turned off. An infrared thermal imaging camera records the temperature at a maximum of 60 frames per second, and the length of the video can be adjusted to capture the entire experimental run. The data acquisition begins while the power supply is still switched off, then after approximately 0.25 seconds the power supply is turned on. As the filament is heated, the amplitude of the phosphor emission intensity decreases. For this phosphor, at a certain temperature well above its sensitivity range, the emission will decrease to a minimum of approximately 10-15% of the maximum emission amplitude. Once the intensity reaches its minimum value or ceases to change amplitude, the data acquisition ends. This process of heating and data aquisition lasts between 1 and 4 seconds, depending on the amount of power supplied to the filament. For a filament rated at 100 watts, the maximum DC voltage applied should not be much more than 9 volts. Above 9 volts, the filament temperature can get high enough to emit light in the visible range, which may be recorded by the photomultiplier tube erroneously.

Visible light emitted from the filament is not a problem in this experiment, as the temperature required for visible light emission is well above the sensitivity range of the 630nm band of La_2O_2S:Eu, but it could be an issue with phosphors with higher sensitivity ranges.

CHAPTER IV

RESULTS

Most of the results from the steady-state portion of the experiment have been presented, as the main purpose is the creation of the calibration curve (recall figure 8). However, a comparison should be made of the standard model to the transient models at steady state. Figure 12 is a plot of the decay time at 190°C. The plot includes the same data from the standard model in figure 7 as well as the decay time data extracted using the power and exponential models. Recall that under steady-state conditions, the power model contains a singularity and the exponential model reduces to the standard model. However, any noise in the emission data results in a non-zero value for $d\tau/dt$, so that the power model may not contain a singularity. Even though the transient models produce results similar to those of the standard model under steady-state conditions, the standard model is still the optimal model to use for determining decay time. Notice that the variation in the values of decay time for the exponential and power models are more than double that of the standard model, as the values of standard deviation are 3.9μs versus 1.7μs, respectively. The exponential and power models have an extra free parameter, so the estimates are less accurate compared to estimates from the standard model. Knowing that the temperature does not change and that the decay time is temperature dependent, a non-zero value for $d\tau/dt$ is incorrect and represents error in the results for decay time. Figure 13 is a plot of the values of $d\tau/dt$ extracted from the data taken at 190°C using the exponential model. The plot shows that there is noise causing non-zero values as well as a non-zero average for $d\tau/dt$. The standard deviation is 0.012, and the average value of $d\tau/dt$ is 0.00031. Although the average value for decay time is almost identical for the three methods, at 257.5μs for the standard model and 257.3μs for the exponential and power models, the standard model is preferred under steady state conditions because there is no additional source of error with a transient term. It

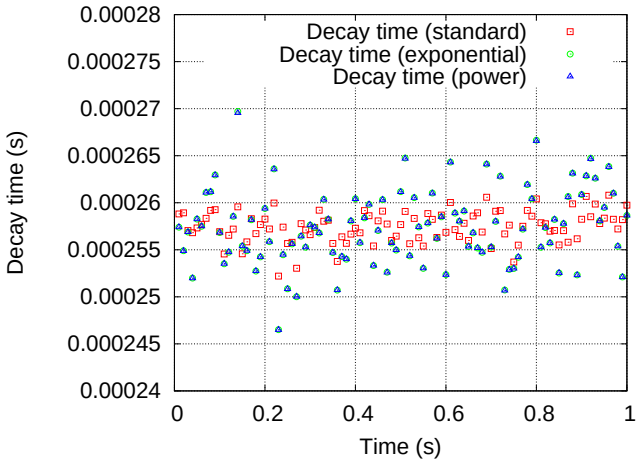

Figure 12: Decay Time at 190°C at Steady-State

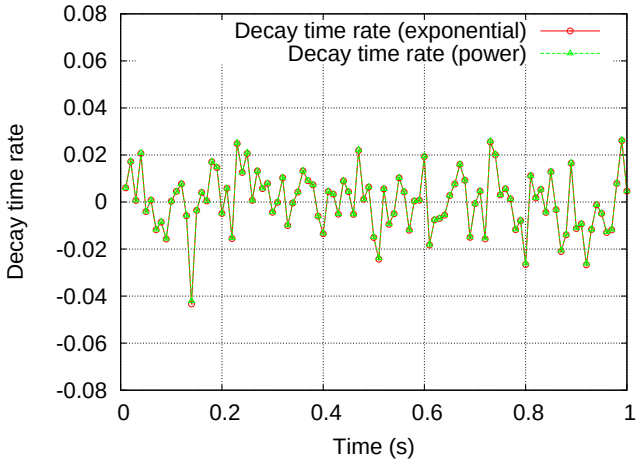

Figure 13: Decay Time Rate at 190°C at Steady-State

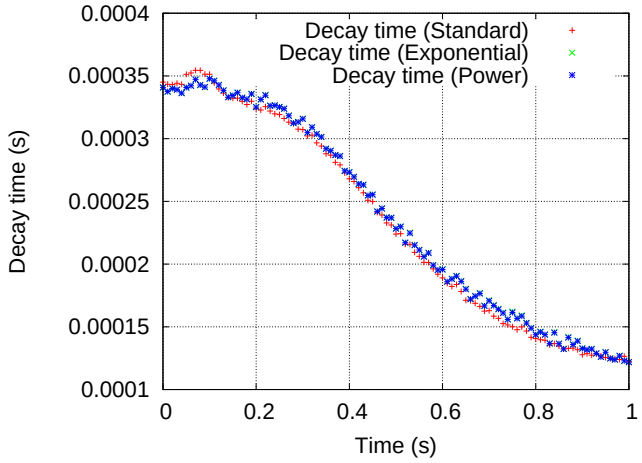

Figure 14: Decay Time, with Filament Heating at 6.4 volts

would then seem appropriate to assume that under transient conditions the standard model is not appropriate, as there is no term to account for the change in decay time as the temperature changes. Figure 14 is a plot of decay time determined from each of the three models as the filament is heated at 6.4 volts. When the filament is supplied with 6.4 volts, it heats the phosphor to over 250°C in one second. During the 0.002 second decay of each pulse, the temperature is increasing enough to change the value of τ. The transient models extract a value for τ at the beginning of the decay with a transient term, $d\tau/dt$, to account for the change in decay time during the decay. The standard model assumes that the decay time is constant over the decay, but the decay time is actually decreasing, so the values of τ from the standard model are lower than the values of τ from the transient models, and this trend can be seen in figure 14. Therefore, when dealing with transient data, only the results from the exponential and power models are accurate.

Figure 15 is a plot of the decay time rate, $d\tau/dt$, taken from the data of filament heating at 6.4 volts using the exponential and power models. As expected from the plot of decay time, the values of $d\tau/dt$ start out positive and quickly become negative, indicating an increase in temperature. However, just past t=0.6 seconds, the values of $d\tau/dt$ decreases further when it appears the slope of figure 14 is in-

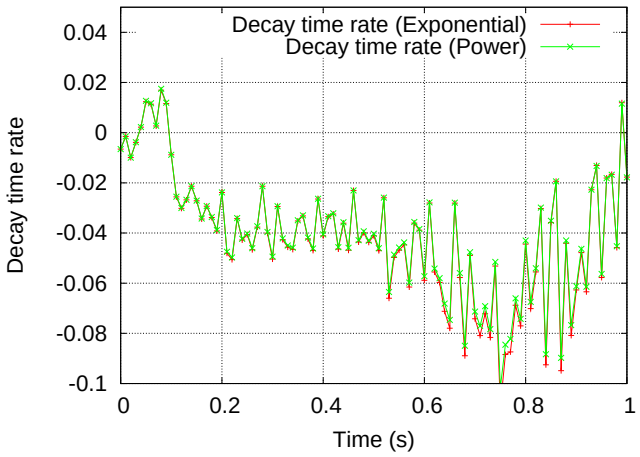

Figure 15: Decay Time Rate, with Filament Heating at 6.4 volts

creasing. Past t=0.8 seconds the value of decay time rate begins to increase as it approaches zero, which is in agreement with the plot of decay time. One explanation for the continued decrease of dτ/dt is that as the temperature increases, the intensity decreases, so that the amplitude of the intensity of the decay is small relative to any noise. Therefore, at higher temperatures, we expect to see a greater effect on the parameters of the curve fit from any noise in the system.

The temperature profile of the filament heated at 6.4 volts is seen in figure 16 as measured with a thermal imaging camera. If the section of interest, which is the portion of the graph between 170°C and 210°C, is treated as a straight line, then the slope can be approximated as 200°C/s during the time $0.32s < t < 0.52s$. We can then use the chain rule from equation 13 to approximate the heating rate using the phosphor data. Looking at the plot of decay time in figure 14, the slope of the line, dτ/dt, between $\tau = 310\mu s$ and $\tau = 210\mu s$, is approximated as -0.000417 s/s. From the calibration curve, dT/dτ is approximately -400,000 °C/s. The product of these two values gives the heating rate as 167 °C/s. A further comparison can be made using dτ/dt taken directly from the measurements as a parameter of the curve fits using the exponential and power models. The average values of dτ/dt are -0.04014 and -0.03953 using the exponential and power models, respectively. Using

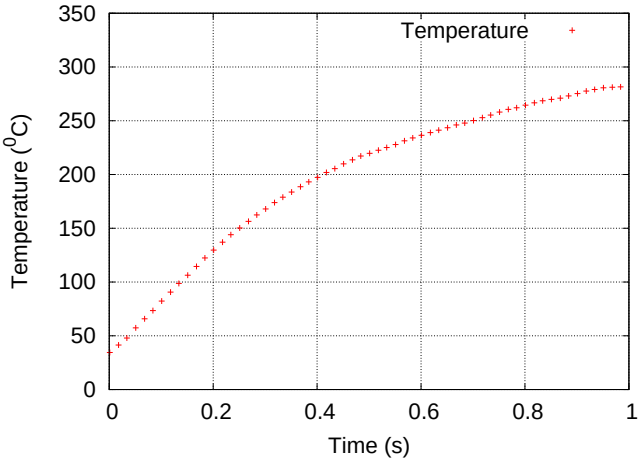

Figure 16: Phosphor Temperature During Filament Heating at 6.4 volts

these values in the chain rule yields heating rates of 16,056°C/s and 15,812°C/s. These values are approximately two orders of magnitude higher than the other two estimates, and this discrepency will be addressed later.

The experiment was run again with a lower voltage of 5.5 volts applied to the filament. The filament heats the phosphor to over 200°C in one second, as seen in Figure 17. If the area of interest, from 170°C to 210°C, is treated as a straight line, then the heating rate is estimated as the slope of figure 17, which is 133°C/s. The intensity data recorded during heating is then analyzed to extract the decay times and decay time rates from the models. The decay times from the three models are shown in figure 18. Recall that the decay times from 310μs to 210μs correspond to temperatures from 170°C to 210°C. From the plot of decay time in figure 18, if the decay times are treated as a straight line in the area of interest, then the slope of that line is 0.000345 s/s. Multiplying the estimated value of dτ/dt by the previously determined value of dT/dτ, which is 400,000 °C/s, the estimated heating rate using the chain rule is 138 °C/s. The decay time rates extracted from the curve fit are displayed in figure 19. The average value of dτ/dt from $t = 0.57s$ to $t = 0.86s$ is -0.03326 for the power model and -0.03189 for the exponential model. Using those values for dτ/dt in the chain rule, the resulting values of heating rate are 13,304°C/s

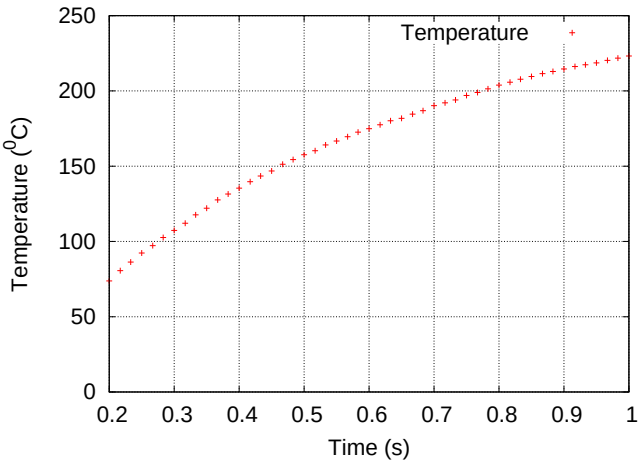

Figure 17: Phosphor Temperature During Filament Heating at 5.5 volts

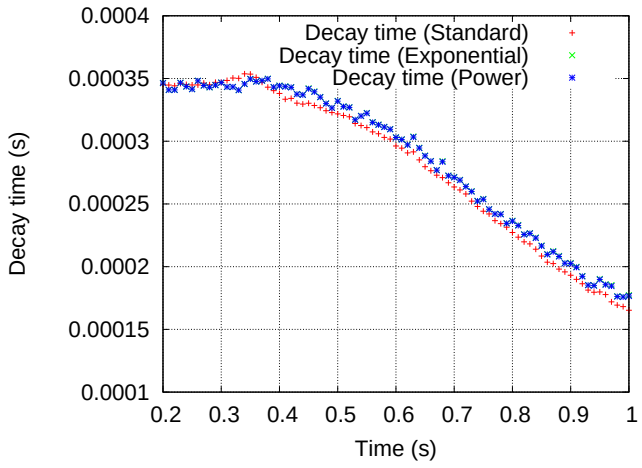

Figure 18: Decay Time, with Filament Heating at 5.5 volts

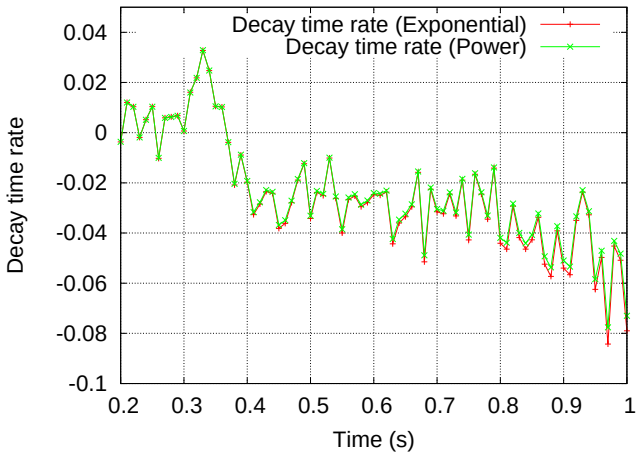

Figure 19: Decay Time Rate, with Filament Heating at 5.5 volts

Table 2: Decay Time Rate, Heating at 6.4 volts

	exponential	power
τ slope	-0.000417	-0.000417
$d\tau/dt$	-0.04014	-0.03953

and 12,756°C/s respectively. Again there is a difference of two orders of magnitude which must be addressed.

In the experiments there were three methods of estimating heating rate. The simplest method, which is used as the standard, is to assume that the temperature increase from 170°C to 210°C is linear, and to use a linear regression to determine the slope of the line, giving the heating rate. The other two methods involve using the chain rule (see equation 13). The $dT/d\tau$ term is found using the calibration curve. The calibration curve (see figure 8) is assumed to be linear, and a linear regression gives the slope as $d\tau/dT$, of which the inverse is taken to determine $dT/d\tau$.

Table 3: Decay Time Rate, Heating at 5.5 volts

	exponential	power
τ slope	-0.000345	-0.000345
$d\tau/dt$	-0.03326	-0.03189

Table 4: Estimated Heating Rates

method	6.4 Volt	5.5 Volt
Camera	200°C/s	133°C/s
decay time slope	167°C/s	138°C/s
decay time rate	16,056°C/s	13,304°C/s

The method of interest, which extracts $d\tau/dt$ directly from the measurement using the power and exponential models, is referred to as the decay time rate method. The other method assumes a linear decrease in the decay time in the region $310\mu s > \tau > 210\mu s$, and uses a linear regression to estimate the slope of the line, which is $d\tau/dt$. This method is referred to as the decay time slope method. Looking first at the case of heating with 6.4 volts, the estimated heating rate using the temperature information from the thermal camera is 200°C/s. The decay time slope method results in an estimate of 167°C/s. This gives a percent difference of almost 18%, which is high, but not unreasonable due to the assumptions of linearly increasing temperature and linearly decreasing decay time in the methods. The decay time rate method results in an estimated heating rate of 16,056°C/s and 15,812°C/s for the exponential and power models. Both of these estimates are two orders of magnitude higher than the other estimates. Notice that although the heating rate estimates are high by two orders of magnitude, it is almost exactly a factor of 100 by which they are too high. If a factor of 100 is taken from the decay time rates extracted using the exponential and power models, then the resulting heating rate estimates are 160°C/s and 158°C/s. Those two heating rate estimates are close to the heating rate estimates for the other two methods.

In the case of heating with 5.5 volts, the estimated heating rate using the temperature from the thermal camera is 133°C/s. The heating rate estimate from the decay time slope method is 138°C/s. The percent difference between these two estimates is 3.7%, which is much smaller than the percent difference in the previous experiment. The heating rate estimates using the decay time rate method are

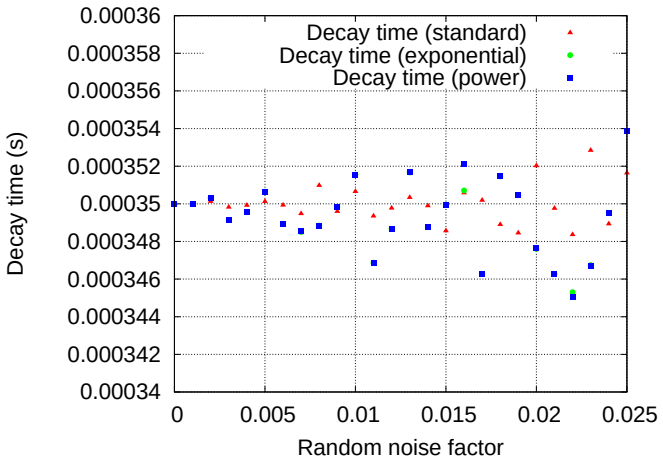

Figure 20: Decay Time Extracted from Simulation

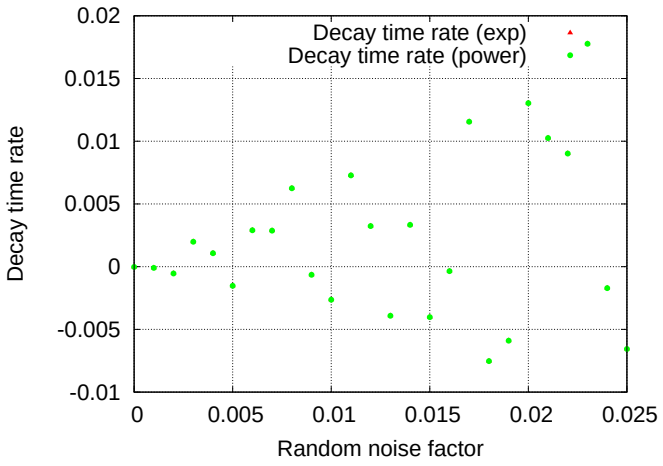

Figure 21: Decay Time Rate Extracted from Simulation

13,304°C/s and 12,756°C/s for the power model and the exponential model respectively. Again, these estimates are two orders of magnitude larger than the other two methods. If a factor of 100 is taken from the values of $d\tau/dt$ extracted from the intensity decay using the power and exponential models, then the estimates for heating rate are 133°C/s and 127°C/s. Those values are close to the estimates found using the other two methods.

In an attempt to understand the error in the results of decay time rate, a simulation of the experiment was performed. In the simulation, fake data is created and noise is added, then a curve fit is performed to extract the known decay time and decay time rate. The parameters are set to $\tau = 0.00035s$ and $d\tau/dt = 0$. Figure 20 shows the results for decay time as the amount of random noise increases. Although the added noise increases the error in decay time, the amount of error is low compared to the values of decay time. The amount of error in the results for decay time in the simulation is comparable to that of the experiment. Now examine the results for decay time rate in figure 21. Recall that in the experiment the expected values of decay time rate were on the order of 0.0004. Notice that even with very small amounts of noise, the error in the results is larger than what the expected results would be for a transient case.

CHAPTER V

CONCLUSIONS

One goal of this experiment was to show that thermographic phosphors can be used for thermometry under transient conditions. The two transient models provide a term to account for the change in temperature, and therefore decay time, during the intensity decay. The standard model is unable to account for the temperature change, and therefore results in an average decay time over the intensity decay. Figures 14 and 18 show that the standard model yields lower values for decay time than the transient models do during heating. The second goal of the experiment was to show that thermographic phosphors can also be used to estimate heating rate using direct measurement. The technique used in this experiment is new and has not been tested before now. This is an original attempt to measure heating rate using thermographic phosphors. Using different methods to estimate heating rate, the values of $d\tau/dt$ extracted from the data using the transient models are too high by a factor of 100. The cause of this error is unclear, and originally was thought to be the result of a factor of 100 somewhere in the curve fit. However, after simulating the experiment with known data and variable added random noise, one apparent cause of error is random noise. If the noise can be reduced to a suitable level, it may be possible to determine whether there are other sources of error. If random noise is the dominating source of error and it can be significantly reduced, this method can be used to determine heating rates for use in the solution for heat flux in the inverse heat conduction problem.

Some sources of error in the experiment that can be improved upon in future trials must be addressed. The use of a laser instead of an LED fully excites the phosphor in a smaller amount of time. It also shuts off immediately when the power is removed, where an LED may have some decay in light emission as the power is removed. Also, the metal housing on the photomultiplier tube forces extra

distance between the photomultiplier tube and the phosphor. If that distance can be minimized, it will increase the magnitude of the emission intensity, resulting in a higher emission to noise ratio. However, it is necessary to keep the metal housing on the photomultiplier tube, as this greatly reduces electrical and optical interference. With these changes in the experiment, the noise can be reduced, which should cause a decrease in error in the results. However, at this time it is unclear how much noise reduction is needed and how much noise reduction is possible.

APPENDIX

PROGRESSION OF DATA COLLECTION

The quality of experimental data in this research has improved dramatically from when the experiments began. Much of the improvement was made with the help of the Thermographic Phosphor Sensing Applications lab at Oak Ridge National Laboratory, specifically Steve Allison. This appendix is meant to show a progression in the quality of data recorded and also to show that the quality of data can continue to progress.

Figure 22 shows a single pulse of phosphor emission recorded at 10,000 Hz. This data was recorded with a photomultiplier tube without aluminum housing. In comparison of this plot to figure 5, the offset is greater here, mainly because there is no housing to shield the photomultiplier tube from electrical and optical interference. This experiment was run under steady state conditions, and the results for decay time and decay time rate are seen in figures 23 and 24. Notice that the values of decay time are significantly different between the transient and steady-state models. Also, the values of decay time rate suggest that the decay time is steadily increasing, which cannot be true at steady-state.

The frequency of intensity readings was increased from 10,000 Hz to 50,000 Hz in the hopes of acquiring better results. Figures 25, 26, and 27 show the emission intensity and the results for decay time and decay time rate under transient conditions. The offset in the emission data is the same as in the 10,000 Hz trials, but the increase in data points increases the accuracy in the curve fits. The results for decay time seem to be accurate early in the heating, but after 0.6 s the decay time begins to increase and the precision decreases greatly. The results for decay time rate seem to agree with those for decay time, as the increase in decay time is accompanied by an increase in decay time rate. However, there is no reason for the decay time to increase as the temperature is decreasing. The error here is due to

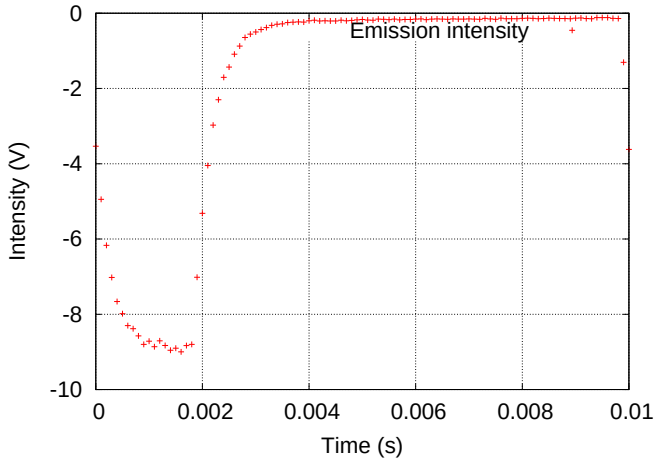

Figure 22: Single Pulse of Emission Data at 10 kHz

optical and electrical interference as the emission intensity decreases. The amplitude of the noise that the interference causes remains constant during the experiment, but as the emission intensity decreases, the interference noise becomes more dominant. The solution is to maximize the emission intensity that the photomultiplier tube records, which can be done in two ways. One method is to increase the amount of phosphor emission, which can be done by increasing the amount of excitation. The excitation can be increased by using a more powerful excitation source, such as a laser instead of an LED, and by minimzing the space between the excitation source and the phosphor. Another method of maximizing the amount of emission recorded is to minimize the space between the phosphor and the photomultiplier tube. Also, the interference noise can be decreased by shielding the photomultiplier tube in an aluminum housing.

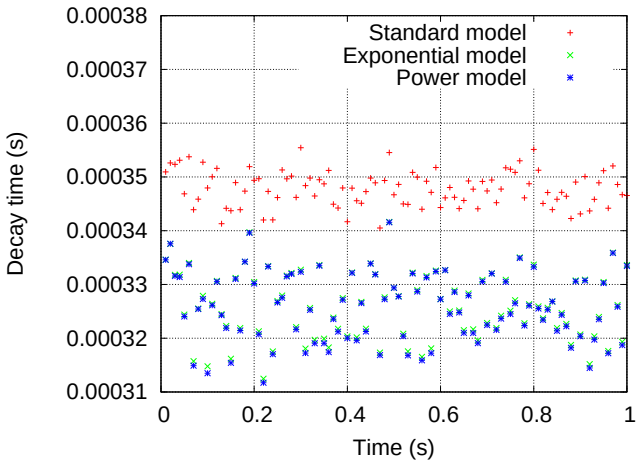

Figure 23: Decay Time Results from 10 kHz Data

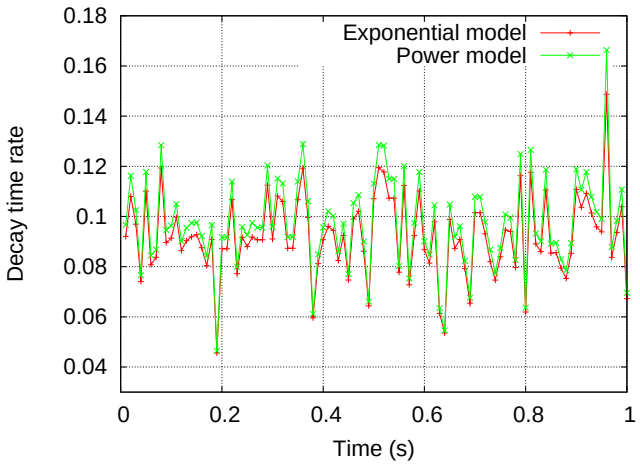

Figure 24: Decay Time Rate Results from 10 kHz Data

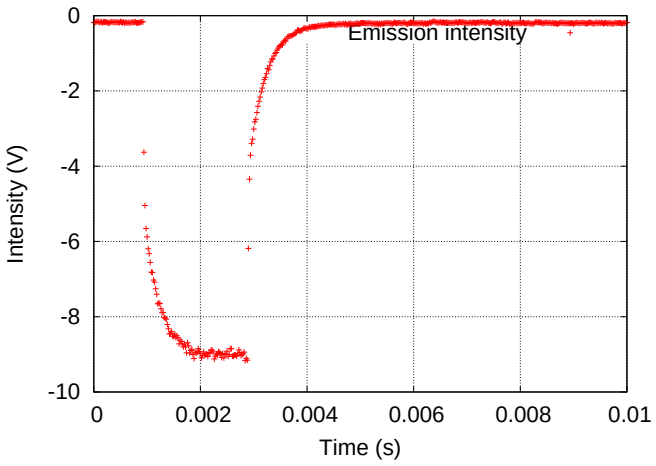

Figure 25: Single Pulse of Emission Data at 50 kHz without Aluminum Shielding

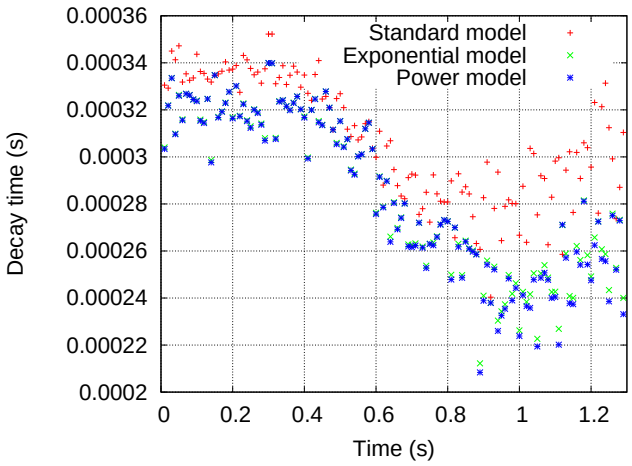

Figure 26: Decay Time Results at 50 kHz without Aluminum Shielding

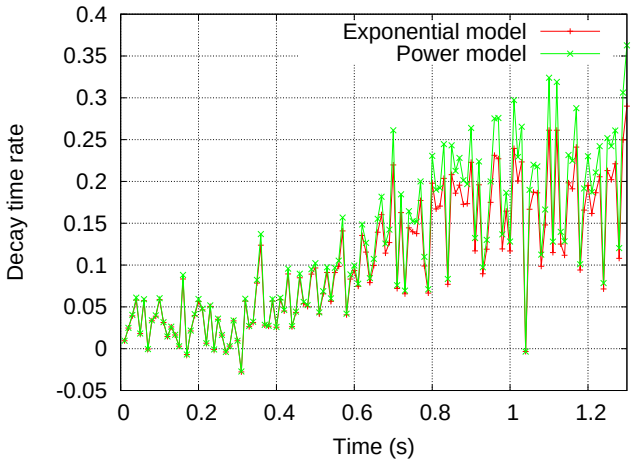

Figure 27: Decay Time Rate Results at 50 kHz without Aluminum Shielding

REFERENCES

S. W. Allison and G. T. Gillies. Remote thermometry with thermographic phosphors: Instrumentation and applications. *Review of Scientific Instruments*, 68(7):2615–2650, July 1997.

J. V. Beck, B. Blackwell, and C. R. St. Claire, Jr. *Inverse Heat Conduction: Ill-Posed Problems*. Wiley-Interscience, 1985.

P. R. N. Childs, J. R. Greenwood, and C. A. Long. Heat flux measurement techniques. *Proceedings of the Institution of Mechanical Engineers Part C-Journal of Mechanical Engineering Science*, 213(7):655–677, 1999.

P. R. Crim, D. G. Walker, S. W. Allison, and S. Goedeke. Reduction of thermographic phosphors data to heat rates. In *proceedings of International Mechanical Engineering Congress and Exposition*, Anaheim, CA, November 2004.

T. E. Diller. *Advances in Heat Transfer*, volume 23, chapter Advances in heat flux measurements, pages 279–353. Academic Press, 1993.

F. F. Ehrich. Differentiation of experimental data using least squares fitting. *Journal of the Aeronautical Sciences*, 22:133–134, 1954.

J. I. Frankel and M. Keyhani. A global time treatment for inverse heat conduction problems. *Journal of Heat Transfer*, 119:673–683, November 1997.

J. I Frankel and M. Keyhani. Inverse heat conduction: The need for heat rate data for design and diagnostic purposes. In *proceedings of the 18th LASTED International Conference on Modeling, Identification and Control*, Innsbruck, Austria, February 1999.

J. I. Frankel and G. E. Osborne. The development of heating/cooling, $\partial T/\partial t$ and heat flux rate, $\partial q''/\partial t$ sensors for aerospace applications. Technical report, Propulsion Measurement Sensor Development Workshop, NASA Marshall Space Flight Center - Space Transportation Directorate, May 2003.

J. P. Holman. *Heat Transfer*. McGraw-Hill, New York, ninth edition, 2002.

R. Kress. *Linear Integral Equations*, volume 82 of *Applied Mathematical Sciences*. Springer-Verlag, 1989.

M. Necati Ozisik and Helcio R. B. Orlande. *Inverse Heat Transfer*. Taylor and Francis, New York, 2000.

S. Shionoya and W. M. Yen, editors. *Phosphor Handbook*. CRC Press, 1999.

A. N. Tikhonov and V. Y. Arsenin. *Solutions of Ill-Posed Problems*. V. H. Winston & Sons, Washington, D. C., 1977.

D. G. Walker. Heat flux determination from measured heating rates using thermographic phosphors. *Journal of Heat Transfer*, 127(6):560–570, June 2005.

D. G. Walker and J. A. Schetz. A new technique for heat flux determination. In *proceeding of the ASME Summer Heat Transfer Conference*, Las Vegas, NV, July 2003.